DFM
Danish National Metrology Institute

Good practice guide for large scale drone based measurements

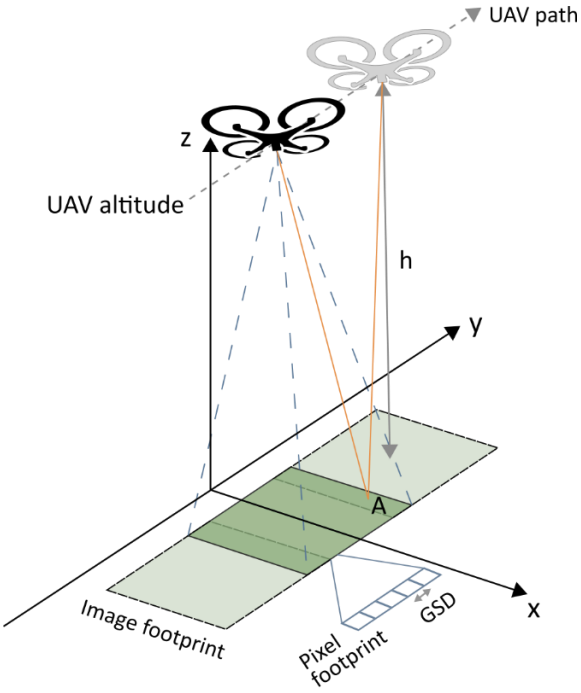

Søren Alkærsig Jensen; Søren A. R. Kynde; Mikkel Schou Nielsen and Jørgen Garnæs

December 2018

Good practice guide for large scale drone based measurements

DFM-PUB 42

2018

By

Søren Alkærsig Jensen; Søren A. R. Kynde; Mikkel Schou Nielsen and Jørgen Garnæs

Published by: Danish Fundamental Metrology A/S, Kogle Allé 5, 2970, Hørsholm

Denmark

Request report

From: www.dfm.dk

Contents

1 Introduction

Unmanned aerial vehicles (UAVs), also known simply as drones, have recently become a popular platform for geomatics [1]. This has been brought about by a recent surge in low cost UAV devices, digital remote sensors and navigation systems. UAV applications offer high ground resolution at low prices [2], and compared to conventional airborne sensing and satellite imaging, particular advantages are found in areas such as heritage locations and rapid response instances [1]. Ongoing UAV research activities are aimed at reducing the size of components, improving navigation, as well as increasing payload capacity and flight times [3].

In this article, we present an overview of the spatial sensing technique that have most commonly been mounted on UAVs. In section 3 we present inherent advantages and drawbacks of each technique, and section 4 contains examples of applications. The focus is on quantitative measurement and the uncertainty of obtained numerical results. Some general considerations about the reliability of results obtained from modern 3D-reconstruction algorithms are given in section 5. Finally, legal issues have the potential to put a stop to some envisioned UAV applications, this is briefly discussed in section 6.

2 The UAV platform

Typical airframes for UAVs are rotary wing (single rotor or multi rotor) fixed wing (unpowered or powered by electric or combustion engine), and lighter than air (balloon or airship). Lighter than air platforms offer almost unlimited flight time and decent payload capacity, but poor mobility. Fixed wing UAVs offer long flight times combined with high mobility, but are unable to remain static or be positioned precisely. The rotary wing platform provides precise positioning combined with a mobility which is typically lower than fixed wing UAVs, and also sacrifices flight time. Rotary drones require more time to perform large scale surveying tasks compared to fixed wing, but find use in cases where high resolution measurements are required, possibly involving a large number of images of an object.

Geomatic areas where UAVs are employed are listed in [1] and include:

- Agriculture, where precision farming can save money and time
- Forestry, where vegetation monitoring, fire surveillance and species identification as well as size estimations can be done
- Archeology and buildings studied with image-based 3D mapping from short distances
- Environmental surveying of land and water, rural areas, and natural resources
- Emergency management, employing UAVs for quick surveying of disaster areas
- Traffic and air pollution surveillance

UAS Denmark is a national industrial drone cluster which serves as a technology sharing network. UAS also provides an international test center located at the H. C. Andersen airport in Odense, Denmark, with geo-referenced ground points, which enables beyond visible line of sight (BVLOS) testing.

UAS devices used for remote sensing are generally operated either manually by a human pilot, or by an autopilot utilizing one or both of two predominant navigation technologies: the Global Navigation Satellite Systems (GNSS) such as GPS, and the inertial navigation system (INS) [4].

The autopilot navigation can be augmented by airspeed sensors, baroaltimeters and magnetometers. A large number of UAS autopilot components are available, some of which are listed in [4]. This system reads the position, attitude and velocity of the UAS, which are passed on to the Flight Control System (FCS). An Orientation System (OS) is generally also used to collect the position and velocity parameters for use in subsequent data analysis. The OS typically provides higher accuracy data, but at a low frequency, as it is not used for real-time navigation. Position data are available from this system on the cm-level [5], its accuracy is limited by the GNSS receiver and antenna [6]. Comparable cm-level precision to that mentioned above can be achieved using georeferencing with cameras when the altitude is 50 m and the ground sampling distance is 2 cm or more. Autonomous flight modes can improve the data quality by ensuring steady elevation, speed and flight direction [7]. GPS provides very accurate spatial data; it falls short in density of data points in many applications [8]. UAV photogrammetry presents an attractive alternative to GPS and total station[1] surveys.

3 Measurement techniques

An increasing number of compact sensor types are available for measurements using UAV platforms [9]. For mapping surface topography and object geometries with UAVs, three main measurement techniques are the camera-based structure-from-motion (SfM) photogrammetry, the laser-based light detection, and ranging (lidar) and the radar-based synthetic aperture radar (SAR).

In the following sections, an introduction to each technique, as well as a discussion of resolution, scan width and sources of uncertainty, will be given.

3.1 Structure from motion

Structure from motion (SfM) is a type of photogrammetry that uses feature correspondences and triangulation for point cloud generation [10]–[12]. As a passive remote sensing technique, SfM relies on natural lighting for its light source. The technique is relatively new within remote sensing. While aerial photogrammetry has been known since the 1920s [13], the origin of SfM stems from developments within computer vision in the 1990s [14]–[16]. SfM was adopted for small UAV platforms in the early 2010s [17]–[21].

In SfM, objects and surfaces are reproduced in 3D by using a set of image acquisitions from different positions and/or camera orientations. These positions and orientations can be very flexible, and SfM allows for a more complicated set of camera viewpoints than standard surveys [17]. The first step of the SfM reconstruction path is the identification of feature points in the individual images. For a number of key feature points or tie points, each point is then located in several images. From these locations, the 3D position of the tie-points is found using a sparse point-cloud triangulation which also determines the pose of the acquisitions [10], [11]. Lastly, a dense point cloud can be created using multi-view stereo (MVS) algorithms. Because of this, the full SfM pipeline can sometimes be referred to as SfM-MVS [22].

[1] A total station (TS) or total station theodolite (TST) is an electronic theodolite used for surveying and building construction

As no knowledge of the camera input positions are required in the SfM pipeline, the produced point cloud in SfM will in general not be to absolute scale. Scaling of the point cloud can be done by including direct georeferenced camera positions from e.g. GPS locations or by georeferencing to externally measured ground-control-points (GCPs) that are identified in the point cloud [20], [23].

One of the reasons for the widespread use of SfM with UAVs is the availability of reconstruction software and low-cost hardware. As it only requires a commercial grade camera for hardware, SfM represents a low-cost technique [12], [22], [24], [25] compared to LiDAR or synthetic aperture radar (SAR). On the software side, a number of commercial SfM solutions are available, including both free, low-cost and high-end solutions [12], [26], [27].

Spectrally, SfM with UAVs is used primarily in the visible range, which allows for applying RGB texture to generated topographies and 3D models. The spectral range can be extended to the near-infrared (NIR) range by integrating multi- and hyperspectral sensors with the SfM workflow [28]. This has been used in a number of studies to determine information on vegetation health and type [29]–[31].

3.1.1 Resolution and scan width

In general, the scan geometry greatly influences the SfM resolution and scan width. As the set of camera views in SfM can be very complicated, the main focus will be on the standard survey geometry shown in Figure 1. Here, the images are assumed to be acquired from a range equal to the flight height *h* and with a constant vertical orientation of the camera.

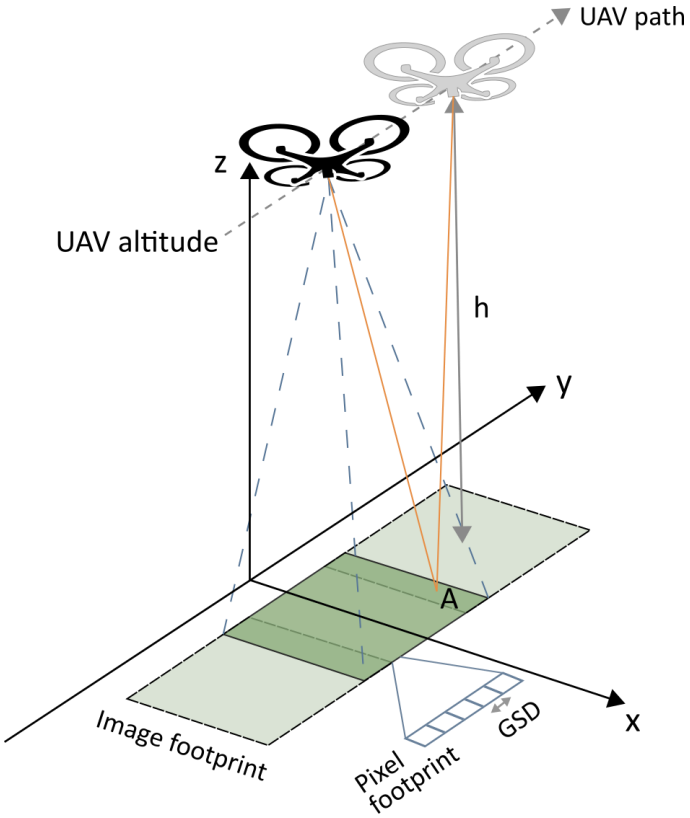

Figure 1 Typical geometry of a SfM survey from a UAV platform.

Overall, the resolution of SfM is limited by the ground sampling distance (GSD) which for digital images is the distance on the ground that a single pixel covers. Assuming a pinhole camera model, the GSD of a vertical looking image can be found from the flight height h, focal distance f of the camera and the physical pixel size of the camera chip d_{px} as

$$\mathrm{GSD} = h \cdot d_{px}/f$$

For a typical UAV flight height of 50 m, a focal length of 25 mm and a pixel size of 5 µm, a GSD in the order of 1 cm is obtained. For very close range imaging at a distance of around 10 m, the GSD shrinks to around 2 mm [32].

While the GSD describes the point spacing on the input images, the resolution of the final point cloud will not be at this level. For detecting each feature that is subsequently reconstructed as a point, a neighborhood of pixels is needed. This results in a lower point density of the point cloud that can typically be an order of magnitude lower than the input images [33], [34]. Thus, for a GSD of 1 cm, the resolution would be in the order of 10 cm.

In survey mode, the smallest detectable height difference δh can be approximated from the parallax between two overlapping images. Compared to a point at ground level, a point A at a height δh will introduce a difference δp in parallax with the following relation [35]

$$\delta h = h \cdot \delta p / p_A$$

where the parallax p_A is the distance on the sensor chip between point A on the two images. For a digital image, the smallest detectable δp is limited by the pixel size d_{px}. The largest possible parallax is obtained when the images have a very small overlap, and A is displaced by the width of the camera sensor equal to the number of pixels N_y times d_{px}. Thus, for a sensor with N_y of 3500 pixels and a flight height of 50 m, the height detection limit will be in the order of 1.4 cm.

The scan width in SfM surveying is given as the swath width (SW) of the image footprint, which is simply the GSD times the number of pixels

$$\mathrm{SW} = \mathrm{GSD} \cdot N_x$$

For a camera chip with 5000 pixels in the cross-track direction and a GSD of 1 cm, a SW of 50 m is obtained.

3.1.2 Sources of uncertainty

The accuracy of SfM reconstructions is influenced by a range of factors related to both the acquisition system and the surface properties of the object.

One main source of uncertainty in SfM surveys stems from the georeferencing by either GCPs or directly by GPS positions [20], [23], [36] if an absolute[2] 3D mapping is intended. Next to georeferencing, the limiting factor in SfM will be the optical resolution given by the GSD. As the GSD of the acquired photos scales with range, the uncertainty contribution in SfM will increase proportionally with the range [11], [24], [37].

As SfM is based on feature extraction from images, object surfaces need to have a level of texture. This texture can either originate from a local variation in surface coloring or a local height variation of the surface topography. A sufficient texture level is required for enough

[2] For an explanation of absolute and relative measurement see section 5.2 *Accuracy of 3D mapping*

distinct features on the object surface to be tracked from image to image [24]. Low texture regions may result in empty regions of the point cloud [20], and could require increased overlap of images [12]. The presence of regions of varying texture can be observed as a variation in point density across the final reconstruction [12], [18], [21], [38].

In the same way, variation in light conditions across a scene may also affect the local point density [36]. In particular, areas with shadows may have a lower point density of the final reconstruction [12], [21], [38].

Since later steps in the SfM pipeline depends on triangulation of feature points, a low angular coverage of the acquired images can be a source of uncertainty, especially for more complicated view geometries. An increase in number of images can improve the accuracy when additional angles and poses are added [22], [39].

3.2 Lidar

Lidar (light detection and ranging) is an active remote sensing technique, which is based on laser ranging for distance measurements [40]. The distance between lidar sensor and target is measured as half the elapsed time between the emission and the detection of a reflected return [41]. A main advantage of lidar systems is for mapping areas with vegetation. By detecting the reflected returns from both the vegetation top and the ground, the height of the vegetation, as well as the bare ground, can be mapped [41]–[43]. This allows for applications within fields such as forest characterization [44], archaeology [45] and agriculture [46].

In the 1980s and 1990s, lidar was adopted for airborne laser scanning with large high-altitude aircraft [47], [48]. Recent developments towards miniature lidar systems with high data rates have allowed for integration with UAV platforms [45], [46], [49]–[52]. With commercial lidar scanners for UAVs becoming available in the last few years, UAV lidar applications are expected to increase [53].

A UAV lidar mapping system consists of three main components: a laser scanner unit to measure the distance to the target; an inertial measurement unit (IMU) to record the pitch, roll and yaw of the platform; and a global positioning system (e.g. a GPS receiver) to record the absolute position of the platform [40], [41]. The laser scanner unit consists of a laser, a detector and a scanning mechanism. Typically, a pulsed semiconductor laser transmitter is used with a wavelength in the range of 800 nm to 1600 nm and pulses of 4 to 15 ns in duration [54]. The scanning mechanism typically uses rotating mirrors to scan the laser beam across the flight track [40]. This is illustrated in Figure 2. The intensity level of the reflected laser pulses in lidar is an additional source of radiometric information. Lidar intensity data have proven beneficial in both data processing and target surface characterization [55].

3.2.1 Resolution and scan width

The resolution and scan width of lidar depend on both internal system properties and the scan geometry. Most often, the scan will be conducted as a standard survey with the platform at a fixed altitude and the lidar facing downwards. However, in some cases, a horizontal scanning direction is preferred [50], [56]. In the survey geometry, the laser beam is scanned in a zig-zag pattern across the ground along the flight path as shown in Figure 2. Each individual laser pulse

creates a laser footprint on the ground from which the reflected signal generates a point in the lidar coordinate system.

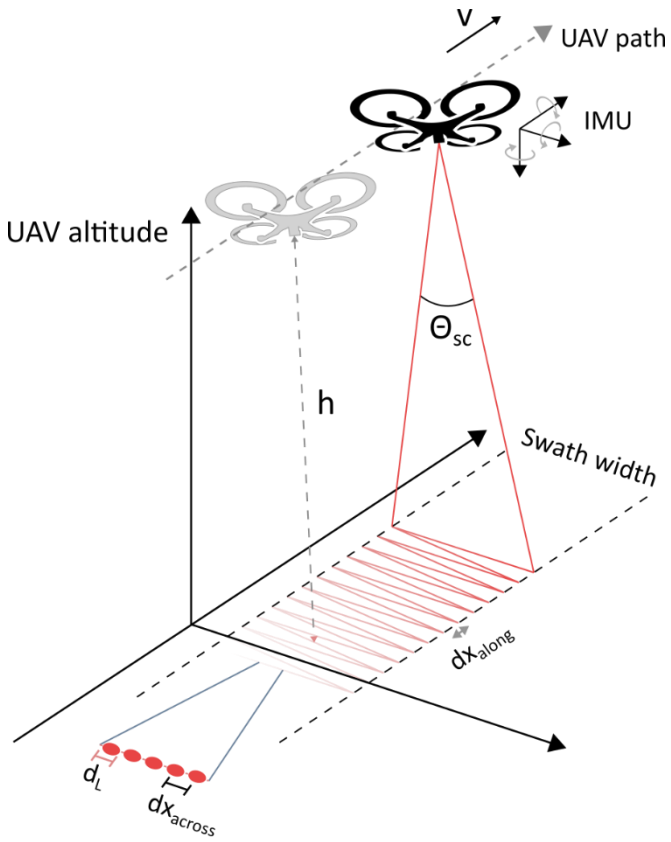

Figure 2 Typical geometry of a lidar survey from a UAV platform.

The vertical resolution of the lidar points is determined by the resolution of the measured distance R. This distance can be found as the speed of light c multiplied with half the time t_R between transmitting and receiving the reflected pulse. Thus, the resolution in distance δ_R is directly proportional to the time resolution δ_t [40]

$$\delta_R = ½ \cdot c \cdot \delta_t$$

With a typical value of δ_t in the order of 0.1 ns [57], δ_R will be in the order of 1.5 cm.

The horizontal ground resolution is limited by several parameters; the laser footprint diameter d_L as well as the point spacing dx across and along the flight direction. The footprint diameter d_L depends on the flight height h, laser beam divergence γ and instantaneous scan angle θ_{inst} [40]

$$d_L = h/\cos(\theta_{inst})^2 \cdot \gamma$$

Assuming that dx_{across} is constant across the swath, an approximation can be made depending on h, the angle range θ_{sc}, the scan rate f_{sc} and the pulse repetition frequency PRF [57]

$$dx_{across} = 2 \cdot h \cdot \tan(\theta_{sc}/2) \cdot f_{sc}/\mathrm{PRF}$$

The point spacing along dx_{along} depends on f_{sc} and the flight speed v [57]

$$dx_{along} = v/f_{sc}.$$

With a UAV flight height of 50 m, a 2 mrad beam divergence, a θ_{sc} of 60°, a f_{sc} of 10 Hz, a PRF of 20 kHz and flight speed v of 5 m/s, the parameters will be on the order of d_L= 10 cm, dx_{across} = 3 cm and dx_{along} = 5 cm. In this example, the laser footprint is the limiting factor for the horizontal resolution. In effect, adjacent reflected pulses will exhibit an overlap. The spacings dx_{across} and dx_{along} will not be equal in general.

The width of the laser scans is determined by the swath width SW. This is given by the flight height h and angle range θ_{sc} as [40]

$$SW = 2 \cdot h \cdot \tan(\theta_{sc}/2)$$

With a UAV flight height of 50 m and θ_{sc} of 60°, SW will be on the order of 60 m.

3.2.2 Sources of uncertainty

Most sources of uncertainty in lidar mapping occur in the transformation from initial points to global coordinates. This transformation adjusts for the platform orientation using the IMU and translates the coordinates to the global position of the aircraft via e.g. GPS. The procedure can be summed up as [58]

$$P_G = P_{GPS} + R_b[R_s r_s - l_b]$$

where P_G are the coordinates of the scanned point in global frame. P_{GPS} are the coordinates of the navigation sensor (the GPS receiver) in global frame. R_b is the rotation matrix from the platform body frame to the global frame via the pitch, roll and yaw angles. R_s is the rotation matrix describing the angular offset between the body frame and the lidar frame. l_b is the translation from lidar position to the origin of the body frame. r_s are the coordinates of the target point given in the lidar frame.

In total, this gives rise to 17 parameters with associated uncertainties [59]. Of these, three are from each of the rotation matrixes R_b and R_s and translation vectors P_{GPS} and l_b. Three additional components are from the lidar system associated with the range measurement and two encoder angles. The last two components arise from the divergence of the laser beam and measurement of elevation angle.

Of these components, the most dominant contribution to the uncertainty comes from the pitch, roll and yaw angles [53], [59]. As these angular contributions scale with distance, the uncertainty in lidar mapping will be worse at higher flight heights [59].

3.3 Synthetic Aperture Radar

Synthetic aperture radar (SAR) is an active remote sensing technique that relies on coherent microwave pulses for image formation. Amongst its main advantages, SAR can produce high resolution images even at long range, and can work in all weather and light conditions both night and day. From the outset in 1960s [60] these properties have made SAR interesting for airborne, as well as satellite platforms [61], [62], beginning with the Seasat mission in 1978 [63]. In recent years, several miniaturized SAR sensors have been developed for use with lightweight UAV platforms [64]–[70].

As any radar system, SAR is an active sensor which emits coherent microwaves from an antenna and processes the returning reflections from the ground into an image. While a

conventional radar image represents an instantaneous snapshot of a scene, SAR uses several detected signals as the sensor moves, to create a composite 2D reflectivity image. The motion of the sensor from the first detected signal to the last results in a “synthetic aperture”, which greatly improves the image resolution compared to using the physical antenna aperture [61]. As a consequence of this motion dependence in image formation, most SAR surveying schemes require a straight-line flight path and stable orientation of the sensor [71].

In addition to 2D reflectivity images, full 3D geometrical mapping of an area can be obtained using images from repeated passes at different incidence angles. In SAR interferometry, the phase-difference from two repeated passes [61], [72] is used to infer the surface topography. From this, a digital elevation model (DEM) can be generated that can be georeferenced for use in GIS applications [62], [73].

Using an even larger number of scans at different heights, SAR tomography can form a full volumetric representation of semi-transparent scenes [74]–[76]. Seeing that UAV platforms are well-suited to perform several passes, three-dimensional SAR mapping with UAVs could well be a useful application. Already, three-dimensional reconstructions from SAR have been reported using UAVs [77]–[79].

Spectrally, SAR operates in microwave frequency bands ranging from the P-band at 0.25-0.5 GHz to the Ka band at 25-40 GHz [61]. For UAV applications, the high-frequency bands such as the X-band (7.5-12 GHz) [68], [77], [80]–[83] and Ku-band (12-17.6 GHz) [84], [85] are the most commonly used. The choice of frequency band determines the penetration depth of the imaged ground (e.g. ice, snow, vegetation, dry soil) [61].

SAR polarimetry provides a way to obtain material information from the reflected signals. By transmitting and receiving in two orthogonal polarizations, the SAR signal can be described by the four elements of a two-by two scattering matrix [61]. One of the applications of SAR polarimetry is measurement of soil moisture under vegetation cover [86], [87] which has been proposed as a use case for UAVs [88].

3.3.1 Resolution and scan width

While the resolution of a SAR system is mostly determined by internal system parameters, the scan width is influenced by the survey geometry. In the typical UAV SAR geometry, the ground is illuminated in a side-looking fashion at a look angle θ_l as illustrated in Figure 3. Coherent microwave pulses are generated by an antenna on the UAV platform and transmitted into an illumination footprint on the ground. After signal processing of the reflected signals, the microwave reflectance can be mapped for each azimuthal and range position.

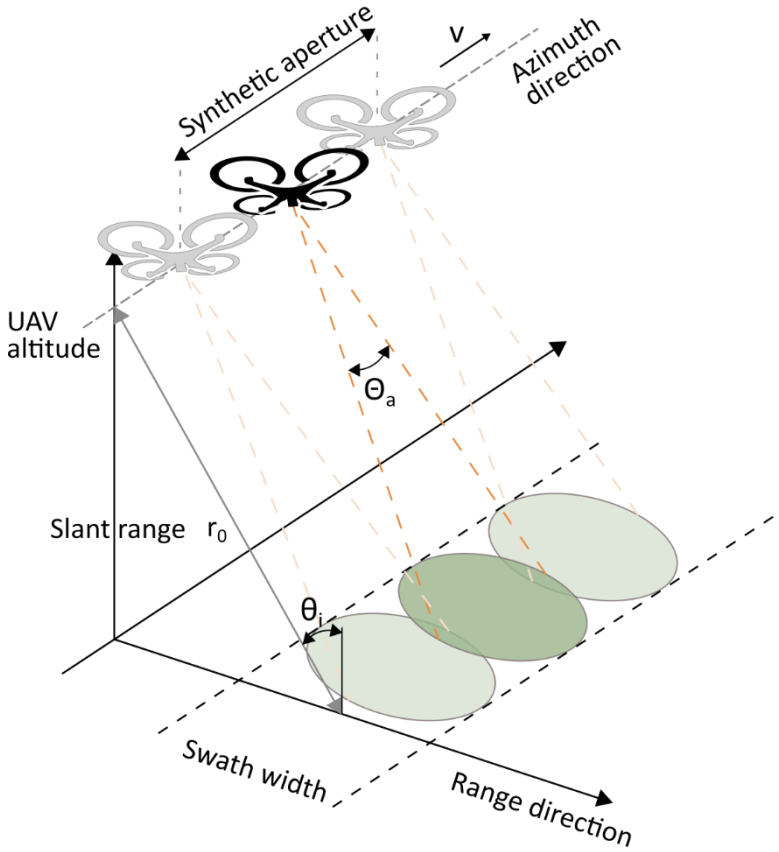

Figure 3 Typical scan geometry of a SAR survey from a UAV platform.

The horizontal resolution in the azimuth and range directions behaves differently. In the azimuth direction, the movement of the platform introduces a Doppler shift in the reflected pulses. By measuring the Doppler shift coherently within a specified Doppler range, the azimuthal position can be determined using several reflected pulses. This constructs a synthetic aperture with a length L_a equal to the path length during which the pulses are received. In a focused SAR mode with a synthetic aperture, the beam pattern narrows, and the azimuthal resolution δ_a becomes [61].

$$\delta_a = \lambda\, r_0/(2\, L_a)$$

Where r_0 is the slant range and λ the microwave wavelength. For a fully focused SAR, the azimuth beam width of a physical antenna of length d_a can be approximated as $\Theta_a = \lambda/d_a$, and the corresponding synthetic aperture length is given as $L_a = r_0\, \Theta_a$. [61] Thus, the theoretical achievable resolution becomes

$$\delta_a = d_a/2$$

which is independent of the range. For typically compact SAR sensors for UAVs, this means potential azimuthal resolutions in the order of 10 cm [77], [83].

In the range direction, the position is determined by recording the pulse echo timing of the transmitted pulse. Conversely, the range resolution δ_r depends on the bandwidth B_r of the microwave pulses as [61]

$$\delta_r = c/2B_r$$

where c is the speed of light. To achieve a sufficiently large bandwidth B_r such that δ_r and δ_a are comparable, frequency modulation schemes are typically applied. A popular approach for UAV applications is to use the frequency modulated continuous wave modulation [68], [70], [77], [80], [89]. UAV SAR systems with bandwidths of more than 1 GHz have recently been reported [82], [83], giving a theoretical achievable range resolution in the order of 10 cm.

In the vertical range, a synthetic aperture in elevation can be established by a vertical flight path with an increasing altitude. Similar to the horizontal resolution, the resolution will depend on the elevation length of the synthetic aperture L_{el} [61]

$$\delta_{el} = \lambda\, r_0/(2\, L_{el})$$

With an aperture length of 3 m and a 10 GHz microwave signal, this gives a theoretical vertical resolution at a range of 200 m in the order of 1 m [77]. For non-vertical flight paths, the resolution will be affected by the elevation angle of the path.

For the scan width SW, the ground swath width of an SAR scan can be calculated from the flight height h, incident angle θ_i and scan angle θ_B as [90]

$$SW = h \cdot (\tan(\theta_i + \theta_B/2) - \tan(\theta_i - \theta_B/2))$$

For h of 50 m and θ_i and θ_B of both 45°, a swath width of 100 m is theoretically achievable.

3.3.2 Sources of uncertainty

One of the largest sources of uncertainty in UAV SAR imaging is the unstable motion of the UAV platform. Compared to satellites or large aircrafts, UAV platforms are more easily disturbed by turbulence due to their small size and light weight [89], [91]. To address this, several motion correction approaches for UAV applications have been implemented [79], [83], [89], [91]–[94]. Due to the limited accuracy of the inertial measurement units and position sensors of UAV platforms, the approaches in general work on the recorded signals rather than external positioning sensors. For highly nonlinear UAV flight paths, approaches to correct for the nonlinearity can also be employed [95], [96].

Another limitation on the accuracy stems from so-called speckle, which arises from the presence of a number of scatterers within a single resolution cell. The coherent nature of the SAR signal leads to a complex reflectivity which depends on both the intensity and phase of the scattered signals [61]. The effect of speckle may be reduced by using a multi-look technique, which has also been applied for UAV applications [97].

4 Applications

The UAV platform can be employed to give valuable information in different applications such as archeological- and geological surveys, urban area monitoring, emergency assistance, etc. [1]. Data in the form of point clouds, polygonal models, and orthoimages are typically produced for these purposes.

4.1 Archeology

In archeological monitoring, precise 3D data is used to link the excavation to the correct historical time, and to digitally document the findings. 3D digitization is commonly employed for cultural heritage preservation [98].

In [99] and [1], an example is given of the Neptune Temple in the archeological area of Paestum in Italy. Both terrestrial and UAV images (vertical and oblique) were used for a SfM 3D reconstruction of the complicated structure. Two flights were performed in autonomous mode using an autopilot system. Flight heights of 130 m for the site, and 70 m for single monuments were used, resulting in average GSDs of 5 cm and 3 cm, respectively [99]. However, the UAV position coordinates were not adequate for direct geo-referencing, and a set of GCPs on corners and features of the structure were found using total stations employing terrestrial laser scanning (TLS). The GCPs provided scaled and geo-referenced 3D results. About 190 ground based- and UAV images were combined and oriented to fit in the same coordinate system; and from this data the camera positions were recovered, and a digital surface model (DSM) was constructed [99].

In another example of UAV aided archeological surveying, the archeological site of Pava, an area of about 60 m by 50 m, was mapped repeatedly during excavation to monitor the volume and follow the progress of the work [1]. Here flights of 35 m height were performed, and an average GSD of 1 cm was achieved. Circular targets measured with a total station were used as GCPs in order to assess the fidelity of the UAV based triangulation results. The RMS errors of the check points for one flight were found to be 3.7 cm in planimetry and 2.3 cm in height [1].

In [98], a comparison was performed between a 3D reconstruction method based on UAV images employing commercial and open source reconstruction software for SfM, and conventional methods such as terrestrial 3D laser scanning and total station measurements. The exterior of the monument Kioutouklou Baba Bekctashic Tekke in Xanthi, Greece was surveyed using terrestrial- and UAV based aerial photography. The 469 terrestrial- and 183 aerial photos were taken at an average distance to object of 4 m. Manual masking of the surroundings of the monument was applied to the images in order to reduce computation time. In the data comparison, laser range scans from 11 positions were taken as ground truth data. For these, an average mean distance between the range scans and the result of the image-based reconstruction was 2 mm with a standard deviation of 14 mm. Comparisons of both methods with distances between points measured with total station also showed good agreement, showing that the image-based reconstruction model does not lead to proportional errors. The image based method did however fail in areas with low frequency color changes and areas lacking strong features [98], this is partially caused by the limit of minimal camera-to-object distance imposed by the UAV.

In geological studies and mining operations, UAVs are an attractive alternative to terrestrial laser scanners because of their ability to perform vertical flights and to produce dense point clouds, which yield detailed information on for instance rock surfaces [1]. UAVs can thus be used for estimating the volume of excavated material in mining areas and quarries.

4.2 Surveying of urban areas and construction sites

In places where regulation allows, UAV based observation can be performed in urban areas. Such areas are typically very complex, and a high number of pictures with high overlap taken at a flight height of 100-200 m, as well as a number of GCPs, are recommended [1].

A densely populated area in Bandung, Indonesia was surveyed with a fixed-wing UAV in [1]. A DSM was created for map fabrication and population estimation. In the area Povo in Trento, Italy, a UAV flight at 100-125 m gave a series of images with an average GSD of about 3 cm and a high level of detail [1]. This was used for extracting building footprints, modeling 3D buildings, and calculating the photovoltaic potential for converting light into electricity.

UAVs are also widely applied to visually monitor construction and operation of a wide range of infrastructure [100]. UAVs can provide large amounts of data to monitor the progress of work, assess safety issues, and inspect structures in areas that cannot readily be accessed by other means [101]. Although autonomous navigation using GPS is commonly used for UAV based land surveying, it has a number of drawbacks when applied to construction sites [100]: It does not account for the continuous change taking place at construction sites, possibly leading to safety hazards, and shadowing effects from nearby structures and steel components can interfere with the navigation. Therefore, manual navigation of UAVs at construction sites is still largely employed. Some of the challenges can be alleviated by making use of an a-priori Building Information Model (BIM) [102]. [100] presents a review of recently applied UAV methods for monitoring of construction sites, buildings and other civil infrastructure.

4.3 Offshore

There are examples of UAVs being used in offshore applications such as oil rigs, shipping and offshore wind turbines. In these areas, UAV based services are still largely regarded as something of an emerging market in Denmark [103]. Barriers to widespread offshore drone application include: The harsh environment which puts strain on the drone and the operator, safety requirements such as ATEX-approval for use in explosive atmospheres, market entry difficulties between small UAS service providers and large potential customers, legislative restrictions on for instance BVLOS flight, and technological limitations such as battery lifetime, navigation, safety and data processing. Despite these barriers, several areas exist where UAVs are already- or can readily be implemented. These include [103]:

- Inspection of confined spaces in ships such as tanks
- surveying oil rigs, bridges and wind turbines for corrosion and other forms of deterioration
- costal monitoring in search and rescue missions or monitoring of immigration or fishing
- gas leak detection from oil rigs or emission from ships
- communication between ships
- delivery of goods, spare parts, and vital equipment or medical supplies at sea

Offshore UAV work is currently done manually by a UAV pilot, but more automated methods are being explored, these largely depend on the ability to fly BVLOS.

4.4 Agriculture and forestry

Hyperspectral cameras and thermal cameras have been widely tested for various agricultural application. The enhanced spectral information from these cameras opens many possibilities to distinguish healthy plants from stressed or crops from weeds[104].

These cameras typically have a lower resolution than RGB-cameras and thus have advantage of the low altitude of UAVs.

In [105] an area of 3000 acres was imaged from an airplane at an altitude of 500 m with hyperspectral and thermal cameras. This resulted in ground sampling distances of 50 cm and 65 cm respectively, which is sufficient for the identification of individual crowns in an olive plantation. In comparison, reference [106] reports ground sampling distances of 1 cm, 4 cm and 9 cm respectively for RGB, multispectral and thermal cameras simultaneously mounted on a UAV at an altitude of 70 m. The improved resolution in the thermal images allowed for filtering out shaded parts of the canopy of wine plants. This leads to a more reliable estimate of the Crop Water Stress Index[104].

Laser scanners come in sizes that can be mounted on UAVs. Though terrestrial laser scanners can obtain high accuracy compared to terrestrial photogrammetry, the opposite is generally the case for the air-borne equivalents. This has to do with the inclusion of ground-control points in camera-based measurements. With these in place, the camera positions can readily be calculated from data. In the case of laser scanners, the accuracy of the measurements is limited by the a-priory knowledge of the position and orientation of the measurement device given by the orientation system.

Laser scanners can be useful for estimating flight height in mapping applications from relatively high altitudes where the direction of the scanner, to a good approximation, can be assumed perpendicular to the ground [107]. Laser scanners are especially useful for mapping areas covered by woods, since some laser light has the ability to penetrate through the canopy [107]. This way, it is possible to detect the height of the ground under the trees. Because the light is partially reflected from the canopy, it is possible to distinguish canopy from stem and ground elements [108] so that the height of the trees can be estimated.

In a direct comparison of airborne laser scanning and SfM applied to mapping of 3D forest landscape features [44], it was found that similar results could be obtained in areas of sparse canopy cover. In more densely covered areas, the advantage of laser scanning became more pronounced. This would merit the choice of the more expensive laser scanner in applications where the vertical distribution of vegetation is of importance.

5 General considerations and best practices

5.1 Accuracy of land surveying

UAV-based aerial surveying usually involves a flight plan and ground control points for georeferencing [1]. Images are then obtained during the flight, and these images can either be used for stitching/mosaicking, or fed into a photogrammetric algorithm for *structure from motion reconstruction* as described in section 3.1. The overlap between recorded images vary depending on the purpose so that a high overlap combined with a small ground sample distance

is used when detailed 3D reconstruction is needed, whereas less overlap is used for coarser surveying. The UAV is commonly observed by a ground control station.

There are two ways to ensure correct scaling and geo-referencing of a model obtained from photogrammetric reconstruction [107]:

- The reconstruction is constrained by pre-determined positions of several Ground Control Points (GCP) known to a better accuracy than required in the final map. From these points, the resection problem can be solved, i.e. the position, orientation and scaling of the photos can be calculated.
- The reconstruction is constrained by known orientation and position of the camera in selected camera locations, together with the focal length and magnification of the camera. This is also known as direct georeferencing.

For most topographic applications, a number of ground control points is used [107]. The minimum number of required control points to solve the resection problem are three vertical and two horizontal points [107]. This determines seven coordinates, corresponding to the seven parameters (position, orientation and scale) of the resection problem. Any extra redundant GCPs offer a way to externally verify the accuracy of the mapping. By excluding some of the redundant GCPs from the reconstruction, their position can be measured on the constructed map and compared to the known ground truth. In the simple geometry of a flat landscape, the verification points can be assumed to be representative for all points in the landscape, and such a verification gives a very strong indication of the accuracy of the map. Note that some authors report the root mean squared error of GCPs that were already included in the reconstruction. This will in general lead to an underestimation of the uncertainty. In principle, the same verification procedure can be established with direct georeferencing, however, it is difficult later to discover general errors or offsets in the information from the orientation system of a particular flight. Finally, it is of course possible to combine ground control with direct georeferencing to create extra redundancy.

The creation of topographic maps in Denmark is governed by national standards [109][110]. The standards specify the quality and density of GCPs and the expected accuracy of the resulting maps, assuming traditional airplane photogrammetry. Topographic maps are routinely made with 7 cm lateral precision based on airplane photos taken from an altitude of 900 m and GCPs determined with an uncertainty of 5 cm [109] and a ground sampling distance of the same order.

With UAVs, it is possible to get much closer, and thereby get a Ground Sampling Distance on the order of millimeters. In that case, the accuracy of the map may no longer be limited by the GSD. With modern SfM algorithms, thousands of tie-points in each image can be identified and matched between images. A resent, and very thorough study [23] showed how photogrammetric factors such as number of images, image quality and lightning conditions become the most critical issues when the resolution is high compared to the GCP accuracy. In this case, validation of the absolute and relative uncertainties of the reconstruction is governed by the same issues as in the reconstruction of complex 3D-shapes.

5.2 Accuracy of 3D mapping

For any 3D mapping, the accuracy or reliability is a key issue, in particular for specifying the measurement capability of a given service provider or the measurement capability of a specific

3D mapping procedure based on the choice of e.g. camera, UAV, distance to the objects, speed of flight, reconstruction software and price. To specify the measurement capability of a 3D mapping, the first step is to identify the exact quantity intended to be measured, that is e.g. a *relative* or an *absolut*e 3D mapping.

The *relative* 3D mapping is a measurement of how objects and surfaces are positioned relative to each other. The accuracy is given by the difference between the reconstructed surface represented in the selected coordinate system and the 'true' representation of the surface in the same coordinate system. When measuring e.g. the distance between two surface points, the (exact) measurement uncertainty is a function of positions of the endpoints on the surface. The measurement uncertainty will in general depend on the magnitude of the distance, but could also be influenced by e.g. the orientation (vertical or horizontal).

Absolute refers to an intended measurement of the objects and surface positions in a geodetic coordinate system that enables every location on Earth to be specified by e.g. latitude, longitude and elevation. The accuracy is given by the difference between the reconstructed surface represented in a geodetic coordinate system, and the 'true' representation of the surface in the same geodetic coordinate system. The uncertainty will typically be different for the latitude, longitude and elevation, and it will always be equal to- or larger than the uncertainty for the relative 3D mapping.

To assess the accuracy, we must assess the inherent uncertainty in e.g. the structure-from-motion (SfM) measurement process and the subsequent software reconstruction due to the limitations in triangulation and image stitching based on distinct observed features such as corner points, color gradients and edges. Possible significant error sources not handled by the surface reconstruction software should also be identified. These errors should be corrected to get the final measured reconstructed surface with no (known) systematic error or other bias. *Possible* significant error sources which are not handled by the software could be:

the uncertainty of the geodetic coordinates of the GCP

the overall scaling of the 3D mapping

outliers, which could be defined as bad points generated when the software misinterprets the data

The overall scaling of the 3D mapping is found from calibration points in the field with e.g. known distance from independent accurate measurements. If not available by other reliable means, the distance could be measured by measuring tape or laser distance sensors with an accuracy of 1 mm for a reasonable cost and effort.

Outliers will probably be most significant for the highest accuracy from UAVs flying close to the surface to be measured. Outliers could be due to lack of contrast on the observed surface, semi-transparent surfaces or highly reflecting (mirror-like) surfaces. From a measurement point of view, these points should be *eliminated* from the reconstructed surface as no measurements have been done. If some interpolation is done, the method and area applied should be reported.

Furthermore, significantly influential parameters should be identified. These could be:

The GSD

The number or area of “poor” surface segments with low or missing contrast from corner points, color gradients or edges

The number of “good” distributed characteristic point that can be used to match the images

Number and position of possible Ground Control Points and/or additional checkpoints in the field which can help reconstruct the surface more accurately

Wind speed and visibility

Strength and stability of the GPS signal

The GSD defines the spatial resolution and depends on the parameters of the camera and the cameras altitude/distance. The accuracy or measurements uncertainty cannot – at least easily - be better that the spatial resolution. However, currently, the best measurement capability is suggested to be in the range of 1-2 $\times$ GSD horizontally and 1-3 $\times$ GSD vertically [111]. This seems to be possible to achieve on a routine basis with good recording conditions on good quality surfaces. Good recording conditions require a good GPS signal, stable flight and decent weather conditions. Surfaces of good quality means many evenly distributed characteristic points that can be used to match the images. For a low or medium cost drone system (as of 2018), flying roughly 100 m from the target, a mean error for target centers of 2.1 cm in XY and 3.1 cm in Z can be achieved [8].

The quantities to be measured could ideally be described in mathematical terms based on the dependency of the different input parameters (e.g. triangulation values, possible GPS and GCP), and the associated measurement uncertainties could ideally be calculated based on the measurements results’ dependency on the input parameters.

As a matter of good practice, any service provider should have control procedures to monitor the validity of the accuracy of the reconstructed surface. The best way to assess the accuracy is probably from several checkpoints in the field with e.g. known distances from independent accurate measurements.

It will improve the value of any 3D reconstruction or measurement based on a 3D reconstruction, if the accuracy and/or uncertainty is quantified and stated in the report. For routine measurements a (conservative) uncertainty could be stated as e.g. a value in cm of the surface position in a geodetic coordinate system. For distances of more than a few meters, the measurement uncertainty could be stated as a particular fraction of the distance such as 0.3 %. It will improve the reliability of any report of 3D reconstruction if the source of overall scaling is stated.

5.3 Improving documentation for reliability

Improved reliability and acceptance of UAV based 3D mapping will create more business for the service providers and benefit costumers and society. Currently (2018), there are no dedicated ISO standards describing norms or requirements regarding 3D mapping by UAV. However, general aspects of geospatial positioning and accuracy are described in standards. The recent publication “A Guide to the Role of Standards in Geospatial Information Management” [112] addresses the role of standards from e.g. the Open Geospatial Consortium (OGC) and ISO in

geospatial information management, and includes a discussion of emerging standards and trends.

A clarification and the mathematical definition of accuracy based on the observed standard deviation of the measured coordinates of checkpoints in the dataset, and the coordinates of the same checkpoint from an independent source of higher accuracy is e.g. given in the Geospatial Positioning Accuracy Standards, Part 3: National Standard for Spatial Data Accuracy [113].

Details of the SfM algorithms in commercial software are most often *not* revealed by the manufacturers, and thus unknown to the service provider. Therefore, the UAV and associated software thus have to be assessed as a “black box” when testing. This means that testing shall be focused on output as function of input and cannot be based on a complete understanding of the underlying calculations and measurements. However, it should be noted that the core principles of the photogrammetric imaging technique for estimating three-dimensional structures from a two-dimensional image sequence are very well discussed and clarified in VDI/VDE guidelines [114], [115].

Below are some definitions, interpretations, clarifications and basic steps which focus on documentation of reliability in the best practice.

Informally, the documentation should ensure that the 3D mapping is good enough with respect to representativeness, reproducibility and repeatability. To more formally document the reliability of mapping, the service provider should *validate* the measurement procedure. The formal steps in a validation is to specify the intended use such as 3D mapping with a given accuracy, and then by examination and objective evidence prove that the specification including the accuracy can be achieved. The specification of the 3D mapping should give the 3D mapping capability in term of a (maximum) range and the associated (best) accuracy in terms of e.g. an uncertainty of the geodetic coordinate or the dimension measured. The specification should be limited to good, but realistic achievable recording conditions with respect to weather and surface conditions. The examination and objective evidence could be a report which documents that the accuracy can be achieved e.g. by measuring some control point with known positions from other sources. The reliability is increased if there are clear and well documented evidence that quantitative limits and tolerances have been met, and the report is approved by a person with sufficient special technical knowledge about the subject.

If the surface is not suitable for accuracy, or the weather condition are not good, the service provider could estimate that the actual accuracy for a task would be lower. It will increase the reliability and acceptance if the report explained the reason for the increased uncertainty.

6 Legal considerations

6.1 Internationally

Legal frameworks for on the UAV sector has been built on the national level since the early 2000s. Current UAV legislation either allow, restrict, or prohibit UAV operation, and often presents a significant barrier to the development of the field [116]. The purpose of the regulations is to minimize risks to people and property both in the air and on the ground. Particular concerns include privacy, data protection and public safety. This legislation is still on an early stage, and national rules vary greatly because of the rapid development of UAV

technology [117], [118]. This represents a great hindrance to the technological development within the UAV field, as well as poor market exploitation [119]. Flight approval times [120] and administrative processes that limit flexibility are examples of legislative problems.

The first legislation concerning UAV was passed in conjunction with the first globally acknowledged aviation principles at the Chicago Convention in 1944 [121]. Here it was specified that no aircraft should be flown without a pilot in a contracting state without a special authorization by that state.

Early UAV regulations were aimed at model aircraft [120], but after years of technological UAV development, the International Civil Aviation Organization (ICAO) called out for international harmonization in the use of civil UAVs in 2012 [122]. At that time, only five countries had introduced UAV regulations. Several countries followed, but about half the countries in the world still did not have UAV regulation in place by 2016 [116].

In their recent manual on remotely piloted aircraft [122], the ICAO made recommendations for the safe operation of UAVs in controlled airspace, considering UAVs as an equal partner in the civil aviation system, able to interact with air traffic control and other aircraft. The organization JARUS, which comprises 49 national authorities and experts, works to harmonize UAV regulation, and recommends that the UAV weight be regulated to be kept below 150 kg. The European Aviation Safety Agency (EASA) published the Riga Declaration on Remotely Piloted Aircraft (Drones) in 2015 [123], specifying five guiding points for European regulations: (1) Drones should be treated as a new type of aircraft fulfilling new rules; (2) there is an urgent need for new EU rules for safe drone operation; (3) Development of technology and standards is needed; (4) public acceptance is an important issue; (5) drone use is the responsibility of the operator. UAV rules developed by EASA generally focus on how the UAV is operated, rather than the specifics of the UAV itself. Beside governmental efforts, the Humanitarian UAV Network (UAViators) comprises more than 2500 members and are involved in developing standards for UAV use.

In [116] a direct comparison between UAV regulation in 19 countries is presented. Numerous differences are revealed, even in the range of devices to which the regulations apply. This is typically determined based on the weight of the UAV, range, or the purpose of the flight (e.g. commercial). Almost all countries specify a maximum weight, which varies between 6 and 150 kg, and most also specify various weight classes with different regulation. 12 out of the 19 countries mentioned in [116] impose special instrument requirements regarding e.g. control systems or safety features such as collision avoidance systems or parachutes. All countries in the survey except Nigeria and Malaysia have defined areas where UAV flight is prohibited, such as airports. Ten countries specify a minimum distance to people, properties and other vehicles, ranging from 30 m to 150 m, and another six countries have issued a general prohibition to fly over crowds of people, leaving only three countries without regulation regarding flying close to people. 12 of the countries also prohibit flight over congested areas such as towns, although the term ‘congested area’ is vaguely defined. Limitations are also put on flight height and horizontal distance. All countries in the survey except China and Nigeria define maximum flying heights, which range between 90 m and 152 m. Such low flying heights serve to separate UAVs from manned aircraft. All 19 countries allow UAV operation within visual line of sight (VLOS), this can in some cases be enhanced to extended visual line of sight (EVLOS) by using an observer on the ground. 13 countries allow flight beyond visual line of sight (BVLOS), often with special conditions such as weight restriction, a need for special approval, or a requirement to fly in

segregated airspace. Eight countries have further restrictions on the maximal horizontal distance ranging between 100 m to 750 m.

The application process required to obtain flight permission generally depends on type of UAV use, but varies greatly between countries. Some countries do not require any application procedure for UAV operation below a certain maximum takeoff weight (MTOW). For instance, Austria, Italy, and Canada do not require approval if the MTOW is below 25 kg. Japan, France, and UK requires application for approval if the flight is to take place in certain areas. Other countries review applications on a case-by-case basis. Local notification and flight approval is also typically employed in order to adhere to local restrictions, prevent conflict with other airspace users or the general public, and to allow monitoring of the flight. This often includes notification to the police and land owners. Notification to air traffic control is required when flying over controlled airspace in practically all cases. Disaster relief UAV or UAVs operated by governmental institutions are often exempt from the aforementioned restrictions. In addition to the application process, several countries also require a separate registration for commercial flight. Liability insurance [119] is also required in most, but not all, countries [116].

In addition to the UAV, restrictions also apply to the UAV pilot. Most common are theoretical and practical skill tests, as well as medical tests. The requirements to the pilot depends on the complexity of the UAV operation. Most countries, with the exception of Japan, UK, Germany and Azerbaijan [116], require a pilot certification or license. Certificates are typically issued by training centers or UAV manufacturers, and involve practical and theoretical training. A license typically requires certain knowledge of aeronautics and involves medical tests. Licenses are generally granted by national aviation authorities.

6.2 Denmark

In Denmark, different rules apply for private- and commercial use of UAVs [124], [125]. All owners of drones heavier than 250 g must acquire a ‘drone sign’, and must enter a registry [126], [127]. The maximum permitted flight height in Denmark is 100 m and 120 m for private- and commercial operation, respectively. A minimum distance of 150 m to buildings, major roads and railroads, and 50 m to persons not involved in the UAV activity, must be kept for all drones above 250 g. It is illegal for private persons to fly over urban areas, and a minimum distance of 150 m to such areas must be respected. Flying over urban areas is allowed for commercial purposes, provided the operator has taken a drone permit [128]. In this case, flights that are considered high risk such as flights BVLOS, indoor flights or autonomous flights, require that a special permit is obtained. Particularly, the restriction on BVLOS flight is considered a significant commercial hindrance by Danish industry [125]. Flight over other densely populated areas is also prohibited, and flights over private residences are in most cases not allowed without the consent of the owner/resident.

Privacy and data protection are important topics in discussions of UAV operation [129], [130]. UAVs can easily be used to record personal data with for instance imaging equipment. This can potentially violate privacy- and data protection rights. Such concerns are not efficiently addressed in current UAV regulations. Most mentions of privacy issues are just advice or they refer to other laws not specific to UAVs.

7 Conclusion

We have reviewed the current state of UAV-based spatial mapping. Options for spatial sensing include laser-based light detection, and ranging (lidar), radar-based synthetic aperture radar (SAR), and a conventional camera coupled with a sophisticated data processing step employing structure from motion (SfM) for 3D reconstruction. The latter approach is the most widespread, probably owing to its flexibility and comparably low equipment cost. Examples of camera equipped UAVs being used for large scale measurements include areas such as agriculture and forestry, where the UAV competes with more traditional approaches of classical cartography. UAVs, however, see new applications in 3-dimensional structures such as archeological sites, urban areas and construction sites. Here UAVs can make use of their ability to collect data from various positions, by e.g. flying vertically, and observing structures from distances down to the meter region. A dense point cloud of 3D position data can therefore be extracted from the large amount of high-resolution images via an SfM algorithm. It is found that combining the SfM generated data with ground control points of well-known position, measured by other means such as ground based laser scanners, can significantly improve the accuracy of the measurement as well as add absolute scaling. Well-defined ground control points can also be used to evaluate the uncertainty of the measurement by considering the distance from these points to the reconstructed 3D surface.

8 References

[1] F. Nex and F. Remondino, “UAV for 3D mapping applications: A review,” *Appl. Geomatics*, vol. 6, no. 1, pp. 1–15, 2014.

[2] J. Zhang, J. Hu, J. Lian, Z. Fan, X. Ouyang, and W. Ye, “Seeing the forest from drones: Testing the potential of lightweight drones as a tool for long-term forest monitoring,” *Biol. Conserv.*, vol. 198, no. March 2016, pp. 60–69, 2016.

[3] T. R. H. Goodbody, N. C. Coops, P. L. Marshall, P. Tompalski, and P. Crawford, “Unmanned aerial systems for precision forest inventory purposes: A review and case study,” *For. Chron.*, vol. 93, no. 01, pp. 71–81, 2017.

[4] I. Colomina and P. Molina, “Unmanned aerial systems for photogrammetry and remote sensing: A review,” *ISPRS J. Photogramm. Remote Sens.*, vol. 92, pp. 79–97, 2014.

[5] M. Rehak, R. Mabillard, and J. Skaloud, “A micro-UAV with the capability of direct georeferencing,” *Int. Arch. Photogramm. Remote Sens. Spat. Inf. Sci.*, vol. XL-1/W2, no. September, pp. 4–6, 2013.

[6] F. van Diggelen, C. Abraham, J. de Salas, and R. Silva, “GNSS Inside Mobile Phones: GPS, GLONASS, QZSS, and SBAS in a Single Chip,” *Insid. GNSS*, pp. 50–60, 2011.

[7] S. Siebert and J. Teizer, “Mobile 3D mapping for surveying earthwork projects using an Unmanned Aerial Vehicle (UAV) system,” *Autom. Constr.*, vol. 41, pp. 1–14, 2014.

[8] P. Barry and R. Coakley, “ACCURACY OF UAV PHOTOGRAMMETRY COMPARED WITH NETWORK RTK GPS.” [Online]. Available: http://www.uav.ie/PDF/Accuracy_UAV_compare_RTK_GPS.pdf. [Accessed: 05-Dec-2018].

[9] N. Mohd Noor, A. Abdullah, and M. Hashim, “Remote sensing UAV/drones and its applications for urban areas: a review,” *IOP Conf. Ser. Earth Environ. Sci.*, vol. 169, no. 1, p. 012003, Jul. 2018.

[10] C. Wu, “Towards Linear-Time Incremental Structure from Motion,” in *2013 International Conference on 3D Vision*, 2013, pp. 127–134.

[11] M. W. Smith, J. L. Carrivick, and D. J. Quincey, “Structure from motion photogrammetry in physical geography,” *Prog. Phys. Geogr. Earth Environ.*, vol. 40, no. 2, pp. 247–275, 2016.

[12] M. J. Westoby, J. Brasington, N. F. Glasser, M. J. Hambrey, and J. M. Reynolds, “‘Structure-from-Motion’ photogrammetry: A low-cost, effective tool for geoscience applications,” *Geomorphology*, vol. 179, pp. 300–314, Dec. 2012.

[13] H. C. Fiske, “Topography from Aerial Photographs,” *Mil. Eng.*, vol. 16, no. 89, pp. 399–408, 1924.

[14] B. Boufama, R. Mohr, and F. Veillon, “Euclidean constraints for uncalibrated reconstruction,” in *(4th) International Conference on Computer Vision*, 1993, pp. 466–470.

[15] M. Spetsakis and J. Y. Aloimonos, “A multi-frame approach to visual motion perception,” *Int. J. Comput. Vis.*, vol. 6, no. 3, pp. 245–255, Aug. 1991.

[16] R. Szeliski and S. B. Kang, “Recovering 3D Shape and Motion from Image Streams Using Nonlinear Least Squares,” *J. Vis. Commun. Image Represent.*, vol. 5, no. 1, pp. 10–28, Mar. 1994.

[17] A. Irschara, V. Kaufmann, M. Klopschitz, H. Bischof, and F. Leberl, “Towards Fully Automatic Photogrammetric Reconstruction Using Digital Images Taken from Uavs,” *ISPRS - Int. Arch. Photogramm. Remote Sens. Spat. Inf. Sci.*, pp. 65–70, 2010.

[18] U. Niethammer *et al.*, “UAV-BASED REMOTE SENSING OF LANDSLIDES,” in *ISPRS - The International Archives of the Photogrammetry, Remote Sensing and Spatial Information Sciences*, 2010, vol. XXXVIII, pp. 496–501.

[19] A. Lucieer, S. Robinson, and D. Turner, “Unmanned Aerial Vehicle (UAV) Remote Sensing for

Hyperspatial Terrain Mapping of Antarctic Moss Beds based on Structure from Motion (SfM) point clouds," in *Proceedings of the 34th International Symposium on Remote Sensing of Environment*, 2011.

[20] S. Harwin and A. Lucieer, "Assessing the accuracy of georeferenced point clouds produced via multi-view stereopsis from Unmanned Aerial Vehicle (UAV) imagery," *Remote Sens.*, vol. 4, no. 6, pp. 1573–1599, 2012.

[21] U. Niethammer, M. R. James, S. Rothmund, J. Travelletti, and M. Joswig, "UAV-based remote sensing of the Super-Sauze landslide: Evaluation and results," *Eng. Geol.*, vol. 128, pp. 2–11, Mar. 2012.

[22] M. Favalli, A. Fornaciai, I. Isola, S. Tarquini, and L. Nannipieri, "Multiview 3D reconstruction in geosciences," *Comput. Geosci.*, vol. 44, pp. 168–176, 2012.

[23] M. R. James, S. Robson, and M. W. Smith, "3-D uncertainty-based topographic change detection with structure-from-motion photogrammetry: precision maps for ground control and directly georeferenced surveys," *Earth Surf. Process. Landforms*, vol. 42, no. 12, pp. 1769–1788, Sep. 2017.

[24] N. Micheletti, J. H. Chandler, and S. N. Lane, "Structure from Motion (SfM) Photogrammetry," in *Geomorphological Techniques*, Online Edi., British Society for Geomorphology Geomorphological Techniques, 2015, pp. 1–12.

[25] M. Sturzenegger and D. Stead, "Close-range terrestrial digital photogrammetry and terrestrial laser scanning for discontinuity characterization on rock cuts," *Eng. Geol.*, vol. 106, no. 3–4, pp. 163–182, Jun. 2009.

[26] T. P. Kersten and M. Lindstaedt, "Image-Based Low-Cost Systems for Automatic 3D Recording and Modelling of Archaeological Finds and Objects," Springer, Berlin Heidelberg, 2012, pp. 1–10.

[27] J. Schöning and G. Heidemann, "Evaluation of Multi-view 3D Reconstruction Software," Springer, Cham, 2015, pp. 450–461.

[28] H. Aasen *et al.*, "Quantitative Remote Sensing at Ultra-High Resolution with UAV Spectroscopy: A Review of Sensor Technology, Measurement Procedures, and Data Correction Workflows," *Remote Sens.*, vol. 10, no. 7, p. 1091, Jul. 2018.

[29] T. Sankey, J. Donager, J. McVay, and J. B. Sankey, "UAV lidar and hyperspectral fusion for forest monitoring in the southwestern USA," *Remote Sens. Environ.*, vol. 195, pp. 30–43, 2017.

[30] F.-J. Mesas-Carrascosa *et al.*, "Assessing Optimal Flight Parameters for Generating Accurate Multispectral Orthomosaicks by UAV to Support Site-Specific Crop Management," *Remote Sens.*, vol. 7, no. 10, pp. 12793–12814, Sep. 2015.

[31] D. Turner *et al.*, "Spatial Co-Registration of Ultra-High Resolution Visible, Multispectral and Thermal Images Acquired with a Micro-UAV over Antarctic Moss Beds," *Remote Sens.*, vol. 6, no. 5, pp. 4003–4024, May 2014.

[32] A. Eltner and D. Schneider, "Analysis of Different Methods for 3D Reconstruction of Natural Surfaces from Parallel-Axes UAV Images," *Photogramm. Rec.*, vol. 30, no. 151, pp. 279–299, 2015.

[33] S. Tavani, A. Corradetti, and A. Billi, "High precision analysis of an embryonic extensional fault-related fold using 3D orthorectified virtual outcrops: The viewpoint importance in structural geology," *J. Struct. Geol.*, vol. 86, pp. 200–210, May 2016.

[34] A. Corradetti, K. McCaffrey, N. De Paola, and S. Tavani, "Evaluating roughness scaling properties of natural active fault surfaces by means of multi-view photogrammetry," *Tectonophysics*, vol. 717, pp. 599–606, Oct. 2017.

[35] P. R. Wolf, B. A. Dewitt, and B. E. Wilkinson, *Elements of photogrammetry with application in*

GIS, 4th ed. McGraw-Hill Education, 2014.

[36] J. Goetz, A. Brenning, M. Marcer, and X. Bodin, “Modeling the precision of structure-from-motion multi-view stereo digital elevation models from repeated close-range aerial surveys,” *Remote Sens. Environ.*, vol. 210, pp. 208–216, Jun. 2018.

[37] M. W. Smith and D. Vericat, “From experimental plots to experimental landscapes: topography, erosion and deposition in sub-humid badlands from Structure-from-Motion photogrammetry,” *Earth Surf. Process. Landforms*, vol. 40, no. 12, pp. 1656–1671, Sep. 2015.

[38] Á. Gómez-Gutiérrez *et al.*, “Comparing Two Photo-Reconstruction Methods to Produce High Density Point Clouds and DEMs in the Corral del Veleta Rock Glacier (Sierra Nevada, Spain),” *Remote Sens.*, vol. 6, no. 6, pp. 5407–5427, Jun. 2014.

[39] T. Y. Nicolas D’Amico, “Accuracy analysis of point cloud modeling for evaluating concrete specimens,” *Proc.SPIE*, vol. 10169. pp. 10169-10169–19, 2017.

[40] A. Wehr and U. Lohr, “Airborne laser scanning—an introduction and overview,” *ISPRS J. Photogramm. Remote Sens.*, vol. 54, no. 2–3, pp. 68–82, Jul. 1999.

[41] M. A. Wulder *et al.*, “Lidar sampling for large-area forest characterization: A review,” *Remote Sens. Environ.*, vol. 121, pp. 196–209, Jun. 2012.

[42] M. L. Clark, D. B. Clark, and D. A. Roberts, “Small-footprint lidar estimation of sub-canopy elevation and tree height in a tropical rain forest landscape,” *Remote Sens. Environ.*, vol. 91, no. 1, pp. 68–89, May 2004.

[43] S. E. Reutebuch, H.-E. Andersen, and R. J. McGaughey, “Light Detection and Ranging (LIDAR): An Emerging Tool for Multiple Resource Inventory,” *J. For.*, vol. 103, no. 6, pp. 286–292, Sep. 2005.

[44] L. Wallace *et al.*, “Assessment of Forest Structure Using Two UAV Techniques: A Comparison of Airborne Laser Scanning and Structure from Motion (SfM) Point Clouds,” *Forests*, vol. 7, no. 12, p. 62, Mar. 2016.

[45] S. Khan, L. Aragão, and J. Iriarte, “A UAV–lidar system to map Amazonian rainforest and its ancient landscape transformations,” *Int. J. Remote Sens.*, vol. 38, no. 8–10, pp. 2313–2330, May 2017.

[46] M. Christiansen *et al.*, “Designing and Testing a UAV Mapping System for Agricultural Field Surveying,” *Sensors*, vol. 17, no. 12, p. 2703, Nov. 2017.

[47] W. B. Krabill, J. G. Collins, L. E. Link, R. N. Swift, and M. L. Butler, “Airborne laser topographic mapping results,” *Photogramm. Eng. Remote Sens.*, vol. 50, no. 6, pp. 685–694, Jun. 1984.

[48] J. L. Bufton, J. B. Garvin, J. F. Cavanaugh, L. A. Ramos-Izquierdo, T. D. Clem, and W. B. Krabill, “Airborne lidar for profiling of surface topography,” *Opt. Eng.*, vol. 30, no. 1, p. 72, 1991.

[49] H. M. Tulldahl and H. Larsson, “Lidar on small UAV for 3D mapping,” in *Electro-Optical Remote Sensing, Photonic Technologies, and Applications VIII; and Military Applications in Hyperspectral Imaging and High Spatial Resolution Sensing II*, 2014, vol. 9250, p. 925009.

[50] R. A. Chisholm, J. Cui, S. K. Y. Lum, and B. M. Chen, “UAV LiDAR for below-canopy forest surveys,” *J. Unmanned Veh. Syst.*, vol. 01, no. 01, pp. 61–68, Dec. 2013.

[51] L. Wallace *et al.*, “Development of a UAV-LiDAR System with Application to Forest Inventory,” *Remote Sens.*, vol. 4, no. 6, pp. 1519–1543, May 2012.

[52] Y. Lin, J. Hyyppa, and A. Jaakkola, “Mini-UAV-Borne LIDAR for Fine-Scale Mapping,” *IEEE Geosci. Remote Sens. Lett.*, vol. 8, no. 3, pp. 426–430, May 2011.

[53] M. Pilarska, W. Ostrowski, K. Bakuła, K. Górski, and Z. Kurczyński, “THE POTENTIAL OF LIGHT LASER SCANNERS DEVELOPED FOR UNMANNED AERIAL VEHICLES- THE REVIEW AND ACCURACY,” *ISPRS - Int. Arch. Photogramm. Remote Sens. Spat. Inf. Sci.*, vol. XLII-2/W2, pp. 87–

95, Oct. 2016.

[54] X. Xiaoye Liu, “Airborne LiDAR for DEM generation: some critical issues,” *Prog. Phys. Geogr.*, vol. 32, no. 1, pp. 31–49, Feb. 2008.

[55] A. Kashani *et al.*, “A Review of LIDAR Radiometric Processing: From Ad Hoc Intensity Correction to Rigorous Radiometric Calibration,” *Sensors*, vol. 15, no. 11, pp. 28099–28128, Nov. 2015.

[56] I. Nikolov and C. Madsen, “LiDAR-based 2D Localization and Mapping System using Elliptical Distance Correction Models for UAV Wind Turbine Blade Inspection,” in *Proceedings of the 12th International Joint Conference on Computer Vision, Imaging and Computer Graphics Theory and Applications*, 2017, pp. 418–425.

[57] E. . Baltsavias, “Airborne laser scanning: basic relations and formulas,” *ISPRS J. Photogramm. Remote Sens.*, vol. 54, no. 2–3, pp. 199–214, Jul. 1999.

[58] C. Glennie *et al.*, “Compact Multipurpose Mobile Laser Scanning System — Initial Tests and Results,” *Remote Sens.*, vol. 5, no. 2, pp. 521–538, Jan. 2013.

[59] L. Wallace, A. Lucieer, D. Turner, and C. Watson, “Error assessment and mitigation for hyper-temporal UAV-borne LiDAR surveys of forest inventory.,” in *Proceedings of SilviLaser 2011, 11th International Conference on LiDAR Applications for Assessing Forest Ecosystems, University of Tasmania, Australia, 16-20 October 2011*, 2011, pp. 1–13.

[60] L. J. Cutrona, W. E. Vivian, E. N. Leith, and G. O. Hall, “A High-Resolution Radar Combat-Surveillance System,” *IRE Trans. Mil. Electron.*, vol. MIL-5, no. 2, pp. 127–131, Apr. 1961.

[61] A. Moreira, P. Prats, M. Younis, G. Krieger, I. Hajnsek, and K. Papathanassiou, “A Tutorial on Synthetic Aperture Radar,” *IEEE Geosci. Remote Sens. Mag.*, no. march, pp. 1–43, 2013.

[62] A. Reigber *et al.*, “Very-High-Resolution Airborne Synthetic Aperture Radar Imaging: Signal Processing and Applications,” *Proc. IEEE*, vol. 101, no. 3, pp. 759–783, 2013.

[63] R. Jordan, “The Seasat-A synthetic aperture radar system,” *IEEE J. Ocean. Eng.*, vol. 5, no. 2, pp. 154–164, Apr. 1980.

[64] J.-T. González-Partida *et al.*, “SAR System for UAV Operation with Motion Error Compensation beyond the Resolution Cell,” *Sensors*, vol. 8, no. 5, pp. 3384–3405, May 2008.

[65] M. Edrich and G. Weiss, “Second-Generation Ka-Band UAV SAR System,” in *2008 38th European Microwave Conference*, 2008, pp. 1636–1639.

[66] H. Essen, W. Johannes, S. Stanko, R. Sommer, A. Wahlen, and J. Wilcke, “High resolution W-band UAV SAR,” in *2012 IEEE International Geoscience and Remote Sensing Symposium*, 2012, pp. 5033–5036.

[67] G. Halcrow *et al.*, “PicoSAR Trials Results,” in *2013 14th International Radar Symposium (Irs), Vols 1 and 2*, 2013, pp. 47–52.

[68] A. Aguasca *et al.*, “ARBRES: Light-Weight CW/FM SAR Sensors for Small UAVs,” *Sensors*, vol. 13, no. 3, pp. 3204–3216, Mar. 2013.

[69] M. Edrich, “Design Overview and Flight Test Results of the Miniaturised SAR Sensor MISAR,” in *European Radar Conference 2004, Amsterdam*, 2004, pp. 205–208.

[70] M. Edwards, D. Madsen, C. Stringham, A. Margulis, B. Wicks, and D. G. Long, “microASAR: A Small, Robust LFM-CW SAR for Operation on UAVs and Small Aircraft,” in *IGARSS 2008 - 2008 IEEE International Geoscience and Remote Sensing Symposium*, 2008, p. V-514-V-517.

[71] D. Blacknell *et al.*, “Geometric accuracy in airborne SAR images,” *Aerosp. Electron. Syst. IEEE Trans.*, vol. 25, no. 2, pp. 241–258, 1989.

[72] R. Bamler and P. Hartl, “Synthetic aperture radar interferometry,” *Inverse Probl.*, vol. 14, no. 4,

pp. R1–R54, Aug. 1998.

[73] L. Ge, X. Li, C. Rizos, and M. Omura, “GPS and GIS Assisted Radar Interferometry,” *Photogramm. Eng. Remote Sens.*, vol. 70, no. 10, pp. 1173–1177, Oct. 2004.

[74] X. X. Zhu and R. Bamler, “Very High Resolution Spaceborne SAR Tomography in Urban Environment,” *IEEE Trans. Geosci. Remote Sens.*, vol. 48, no. 12, pp. 4296–4308, Dec. 2010.

[75] F. Lombardini and A. Reigber, “Adaptive spectral estimation for multibaseline SAR tomography with airborne L-band data,” in *IGARSS 2003. 2003 IEEE International Geoscience and Remote Sensing Symposium. Proceedings (IEEE Cat. No.03CH37477)*, 2003, vol. 3, pp. 2014–2016.

[76] A. Reigber and A. Moreira, “First demonstration of airborne SAR tomography using multibaseline L-band data,” *IEEE Trans. Geosci. Remote Sens.*, vol. 38, no. 5, pp. 2142–2152, 2000.

[77] M. Lort, A. Aguasca, C. Lopez-Martinez, and T. M. Marin, “Initial Evaluation of SAR Capabilities in UAV Multicopter Platforms,” *IEEE J. Sel. Top. Appl. Earth Obs. Remote Sens.*, vol. 11, no. 1, pp. 127–140, Jan. 2018.

[78] H. Kuang, J. Chen, W. Yang, W. Liu, and X. Zhu, “Fully three-dimensional UAV SAR imaging with multi-azimuth-angle observation,” in *2017 IEEE International Geoscience and Remote Sensing Symposium (IGARSS)*, 2017, pp. 470–473.

[79] I. Fletcher, C. Watts, E. Miller, and D. Rabinkin, “Minimum entropy autofocus for 3D SAR images from a UAV platform,” in *2016 IEEE Radar Conference (RadarConf)*, 2016, pp. 1–5.

[80] C. Bhattacharya, A. Roy, S. Navneet, A. Heddallikar, and R. Pinto, “MicroSAR: Calibration of X-band high resolution FMCW synthetic aperture radar (SAR),” in *2014 IEEE International Microwave and RF Conference (IMaRC)*, 2014, pp. 377–380.

[81] M. A. Remy, K. A. C. de Macedo, and J. R. Moreira, “The first UAV-based P- and X-band interferometric SAR system,” in *2012 IEEE International Geoscience and Remote Sensing Symposium*, 2012, pp. 5041–5044.

[82] W. Li, H. Zhang, and O. L. Osen, “A UAV SAR Prototype for Marine and Arctic Application,” in *Volume 7B: Ocean Engineering*, 2017, p. V07BT06A002.

[83] Z. Xu and D. Zhu, “High-resolution miniature UAV SAR imaging based on GPU Architecture,” *J. Phys. Conf. Ser.*, vol. 1074, no. 1, p. 012122, Sep. 2018.

[84] L. Weixian *et al.*, “Premier results of the multi-rotor based FMCW synthetic aperture radar system,” in *2016 IEEE Radar Conference (RadarConf)*, 2016, pp. 1–4.

[85] W. X. Liu, H. C. Feng, S. Y. Aye, B. P. Ng, and Y. L. Lu, “Design and testing of multi-rotor UAV full-pol SAR system,” in *International Conference on Radar Systems (Radar 2017)*, 2017.

[86] I. Hajnsek, T. Jagdhuber, H. Schon, and K. P. Papathanassiou, “Potential of Estimating Soil Moisture Under Vegetation Cover by Means of PolSAR,” *IEEE Trans. Geosci. Remote Sens.*, vol. 47, no. 2, pp. 442–454, Feb. 2009.

[87] M. El Hajj *et al.*, “Soil moisture retrieval over irrigated grassland using X-band SAR data,” *Remote Sens. Environ.*, vol. 176, pp. 202–218, Apr. 2016.

[88] K. S. Lyalin, A. A. Biryuk, A. Y. Sheremet, V. K. Tsvetkov, and D. V. Prikhodko, “UAV synthetic aperture radar system for control of vegetation and soil moisture,” in *2018 IEEE Conference of Russian Young Researchers in Electrical and Electronic Engineering (EIConRus)*, 2018, pp. 1673–1675.

[89] Mengdao Xing, Xiuwei Jiang, Renbiao Wu, Feng Zhou, and Zheng Bao, “Motion Compensation for UAV SAR Based on Raw Radar Data,” *IEEE Trans. Geosci. Remote Sens.*, vol. 47, no. 8, pp. 2870–2883, Aug. 2009.

[90] J. Li *et al.*, “Sensor-Oriented Path Planning for Multiregion Surveillance with a Single Lightweight

UAV SAR," *Sensors*, vol. 18, no. 2, p. 548, Feb. 2018.

[91] L. Zhang, M. Hu, G. Wang, and H. Wang, "Range-Dependent Map-Drift Algorithm for Focusing UAV SAR Imagery," *IEEE Geosci. Remote Sens. Lett.*, vol. 13, no. 8, pp. 1158–1162, Aug. 2016.

[92] L. Zhang, J. Sheng, M. Xing, Z. Qiao, T. Xiong, and Z. Bao, "Wavenumber-domain autofocusing for highly squinted UAV SAR imagery," *IEEE Sens. J.*, vol. 12, no. 5, pp. 1574–1588, 2012.

[93] S. Zhou, L. Yang, L. Zhao, and G. Bi, "Forward Velocity Extraction From UAV Raw SAR Data Based on Adaptive Notch Filtering," *IEEE Geosci. Remote Sens. Lett.*, vol. 13, no. 9, pp. 1211–1215, Sep. 2016.

[94] S. Zhou, L. Yang, L. Zhao, and G. Bi, "Quasi-Polar-Based FFBP Algorithm for Miniature UAV SAR Imaging Without Navigational Data," *IEEE Trans. Geosci. Remote Sens.*, vol. 55, no. 12, pp. 7053–7065, Dec. 2017.

[95] O. Frey, C. Magnard, M. Ruegg, and E. Meier, "Focusing of Airborne Synthetic Aperture Radar Data From Highly Nonlinear Flight Tracks," *IEEE Trans. Geosci. Remote Sens.*, vol. 47, no. 6, pp. 1844–1858, Jun. 2009.

[96] Z. Li *et al.*, "A Frequency-Domain Imaging Algorithm for Highly Squinted SAR Mounted on Maneuvering Platforms With Nonlinear Trajectory," *IEEE Trans. Geosci. Remote Sens.*, vol. 54, no. 7, pp. 4023–4038, Jul. 2016.

[97] S. Y. Aye, W. Liu, H. Feng, and B. P. Ng, "Study of multi-rotor UAV SAR processing," in *2017 IEEE Radar Conference (RadarConf)*, 2017, pp. 0226–0232.

[98] A. Koutsoudis, B. Vidmar, G. Ioannakis, F. Arnaoutoglou, G. Pavlidis, and C. Chamzas, "Multi-image 3D reconstruction data evaluation," *J. Cult. Herit.*, vol. 15, no. 1, pp. 73–79, Jan. 2014.

[99] F. Fiorillo, B. Jiménez Fernández-Palacios, F. Remondino, and S. Barba, "3d Surveying and modelling of the Archaeological Area of Paestum, Italy," *Virtual Archaeol. Rev.*, vol. 4, no. 8, p. 55, 2013.

[100] Y. Ham, K. K. Han, J. J. Lin, and M. Golparvar-Fard, "Visual monitoring of civil infrastructure systems via camera-equipped Unmanned Aerial Vehicles (UAVs): a review of related works," *Vis. Eng.*, vol. 4, no. 1, pp. 1–8, 2016.

[101] P. Liu *et al.*, "A review of rotorcraft unmanned aerial vehicle (UAV) developments and applications in civil engineering," *Smart Struct. Syst.*, vol. 13, no. 6, pp. 1065–1094, 2014.

[102] S. Tuttas, A. Braun, A. Borrmann, and U. Stilla, "Acquisition and Consecutive Registration of Photogrammetric Point Clouds for Construction Progress Monitoring Using a 4D BIM," *PFG*, vol. 85, no. 1, pp. 3–15, 2017.

[103] M. H. Frederiksen and M. P. Knudsen, "Drones for offshore and maritime missions: Opportunities and barriers," *SDU Cent. Integr. Innov. Manag.*, 2018.

[104] H. G. Jones and R. A. Vaughan, *Remote Sensing of Vegetation: Principles, Techniques, and Applications*. Oxford University Press: Oxford, UK, 2010.

[105] R. Calderón, J. A. Navas-Cortés, and P. J. Zarco-Tejada, "Early detection and quantification of verticillium wilt in olive using hyperspectral and thermal imagery over large areas," *Remote Sens.*, vol. 7, no. 5, pp. 5584–5610, 2015.

[106] A. Matese and S. Di Gennaro, "Practical Applications of a Multisensor UAV Platform Based on Multispectral, Thermal and RGB High Resolution Images in Precision Viticulture," *Agriculture*, vol. 8, no. 7, p. 116, 2018.

[107] P. Wolf, B. Dewitt, and E. Mikhail, *Elements of Photogrammetry with Applications in GIS*, 4'th Editi. New York: Mc Graw Hill Education, 2014.

[108] B. Brede *et al.*, "Comparing RIEGL RiCOPTER UAV LiDAR Derived Canopy Height and DBH with

Terrestrial LiDAR," *Sensors*, vol. 17, no. 10, p. 2371, Oct. 2017.

[109] C. Pannicelli and F. Hjorth, "Specifikationer for tekniske kort (TK99)," 1999.

[110] B. H. Damsgaard, "Geo Danmark, Specifikation 6.0," 2018.

[111] A. Buczkowski, "How accurate is your drone survey? Everything you need to know." [Online]. Available: http://geoawesomeness.com/accurate-drone-survey-everything-need-know/. [Accessed: 05-Dec-2018].

[112] "A Guide to the Role of Standards in Geospatial Information Management." [Online]. Available: http://ggim.un.org/meetings/GGIM-committee/8th-Session/documents/Standards_Guide_2018.pdf. [Accessed: 03-Dec-2018].

[113] Federal Geographic Data Committee, "Geospatial Positioning Accuracy Standards Part 3: National Standard for Spatial Data Accuracy," 1998.

[114] VDI/VDE, "Optical 3D-measuring systems. Part 2: Optical systems based on area scanning." 2012.

[115] VDI/VDE, "Optical 3D-measuring systems. Part 3: Multiple view systems based on area scanning." 2008.

[116] C. Stöcker, R. Bennett, F. Nex, M. Gerke, and J. Zevenbergen, "Review of the current state of UAV regulations," *Remote Sens.*, vol. 9, no. 5, p. 459, 2017.

[117] A. C. Watts, V. G. Ambrosia, and E. A. Hinkley, "Unmanned aircraft systems in remote sensing and scientific research: Classification and considerations of use," *Remote Sens.*, vol. 4, no. 6, pp. 1671–1692, 2012.

[118] P. van Blyenburgh, "Harmonising UAS Regulations and Standards," *GIM Int. - UAS Spec. Issue*, vol. 30, 2016.

[119] P. Boucher, "Domesticating the Drone: The Demilitarisation of Unmanned Aircraft for Civil Markets," *Sci. Eng. Ethics*, vol. 21, pp. 1393–1412, 2014.

[120] A. Rango and A. S. Laliberte, "Impact of flight regulations on effective use of unmanned aircraft systems for natural resources applications," *J. Appl. Remote Sens.*, vol. 4, no. 1, p. 043539, 2010.

[121] International Civil Aviation Organization (ICAO), "The Convention on International Civil Aviation," 1944, no. December.

[122] ICAO, *Manual on Remotely Piloted Aircraft Systems (RPAS)*, no. April. 2012.

[123] European Aviation Safety Agency (EASA), "RIGA DECLARATION ON REMOTELY PILOTED AIRCRAFT (drones) 'FRAMING THE FUTURE OF AVIATION.'" 2015.

[124] "https://droner.dk/regler-for-droneflyvning." .

[125] J. Villadsen, S. F. Østergaard, and J. Sylvest, "Regulering af droner i Danmark og internationalt," *Teknol. Inst.*, 2017.

[126] "http://www.trafikstyrelsen.dk/da/droneregler." .

[127] Transport- Bygnings- og Boligministeriet, "Bekendtgørelse om flyvning med droner uden for bymæssigt område," *BEK nr 1257 af 24/11/2017*, no. november, pp. 1–8, 2017.

[128] Transport- Bygnings- og Boligministeriet, "Bekendtgørelse om flyvning med droner i bymæssigt område," *BEK nr 1256 af 24/11/2017*, pp. 1–15, 2017.

[129] W. van Wegen and J. Stumpf, "Bringing a New Level of Intelligence to UAVs—Interview with Jan Stumpf," *GIM Int. Interviews*, 2016.

[130] L. B. Moses, "Recurring Dilemmas : The Law's Race to Keep up with Technological Change," *UNSW Law Res. Pap.*, vol. 21, 2007.

9 Acknowledgements

DFM A/S acknowledges funding from the Danish Agency for Institutions and Educational Grants as part of the result contract “Dronemetrologi”.